Chemorepulsion by blood S1P regulates osteoclast precursor mobilization and bone remodeling in vivo

Masaru Ishii,[1,2] Junichi Kikuta,[1] Yutaka Shimazu,[1] Martin Meier-Schellersheim,[3] and Ronald N. Germain[2,3]

[1]Laboratory of Biological Imaging, WPI-Immunology Frontier Research Center, Osaka University, Osaka 565-0871, Japan
[2]Lymphocyte Biology Section, Laboratory of Immunology, and [3]Program in Systems Immunology and Infectious Disease Modeling, National Institute of Allergy and Infectious Diseases, National Institutes of Health, Bethesda, MD 20892

Sphingosine-1-phosphate (S1P), a lipid mediator enriched in blood, controls the dynamic migration of osteoclast (OC) precursors (OPs) between the blood and bone, in part via the S1P receptor 1 (S1PR1) which directs positive chemotaxis toward S1P. We show that OPs also express S1PR2, an S1P receptor which mediates negative chemotaxis (or chemorepulsion). OP-positive chemotaxis is prominent in gradients with low maximal concentrations of S1P, whereas such behavior is minimal in fields with high maximal S1P concentrations. This reverse-directional behavior is caused by S1PR2-mediated chemorepulsion acting to override S1PR1 upgradient motion. S1PR2-deficient mice exhibit moderate osteopetrosis as a result of a decrease in osteoclastic bone resorption, suggesting that S1PR2 contributes to OP localization on the bones mediated by chemorepulsion away from the blood where S1P levels are high. Inhibition of S1PR2 function by the antagonist JTE013 changed the migratory behavior of monocytoid cells, including OPs, and relieved osteoporosis in a mouse model by limiting OP localization and reducing the number of mature OCs attached to the bone surface. Thus, reciprocal regulation of S1P-dependent chemotaxis controls bone remodeling by finely regulating OP localization. This regulatory axis may be promising as a therapeutic target in diseases affecting OC-dependent bone remodeling.

CORRESPONDENCE
Masaru Ishii:
mishii@ifrec.osaka-u.ac.jp
OR
Ronald N. Germain:
rgermain@niaid.nih.gov

Abbreviations used: OC, osteoclast; OP, OC precursor; S1P, sphingosine-1-phosphate; S1PR1, S1P receptor 1.

Osteoclasts (OCs) are a specialized cell subset with bone-resorbing capacity that plays a critical role in normal bone homeostasis (bone remodeling), degrading old bones and facilitating new bone formation by osteoblasts (Teitelbaum, 2000). OCs are differentiated from monocyte/macrophage-lineage hematopoietic precursor cells, termed OC precursors (OPs), and previous studies have revealed key molecular signals, such as those mediated by M-CSF and RANKL, that regulate OC differentiation (Karsenty and Wagner, 2002; Teitelbaum and Ross, 2003). In contrast to the detailed information available concerning molecular signals for differentiation of OC, the factors controlling migration and localization of OPs onto the bone surface, the site of OC terminal differentiation, are less well analyzed. We have recently used intravital two-photon microscopy to visualize the bone cavity in live mice, and found that sphingosine-1-phosphate (S1P), a lipid mediator enriched in blood, plays a critical role in controlling the residence stability of OPs on the bone surface via the cognate receptor S1P receptor 1 (S1PR1; also designated $S1P_1$ or Edg-1; Ishii et al., 2009; Klauschen et al., 2009). The mechanisms controlling the initial localization of OPs into the bone space or counteracting the tendency of S1P to promote movement of OPs from bone to blood, however, have not yet been clarified. In this paper, we show that bone attraction is also contributed to in part by S1P, through a distinct but related receptor, S1PR2 (also designated as $S1P_2$ or Edg-5).

Although both S1PR1 and S1PR2 belong to the heptahelical heterotrimeric G protein–coupled Edg receptor family, their signal

The Rockefeller University Press $30.00
J. Exp. Med. Vol. 207 No. 13 2793-2798
www.jem.org/cgi/doi/10.1084/jem.20101474

The Journal of Experimental Medicine

transduction pathways are completely different (Takuwa, 2002; Rosen and Goetzl, 2005). S1PR1 (via its associated $G_i\alpha$ subunit) activates the small G protein Rac and induces positive chemotaxis. In contrast, S1PR2 (signaling through $G_{12/13}\alpha$) activates another small G protein, Rho. Active Rho can inhibit activation of Rac, which can limit S1P-induced chemotaxis (Fig. 1 A). It was previously reported that S1PR2-expressing cells show reduced migration to S1P in vitro (Okamoto et al., 2000).

RESULTS AND DISCUSSION

We found that OPs express S1PR2 as well as S1PR1, and the positive migratory response to S1P was highly concentration dependent, being more vigorous at low S1P concentrations ($<10^{-7}$ M) and less marked at higher concentrations (Fig. 1 B). In addition, blockade of S1PR1 signaling with pertussis toxin led to a reduction in migration below the basal level seen in the absence of S1P, suggesting that S1P could have a negative effect on cell migration under these conditions. We also found that S1PR2 deficiency enhanced positive S1P chemotaxis. To better analyze the effects of varying S1P concentrations on migration, we examined the dynamics of S1P chemotaxis in an in vitro image-based system (Fig. 1, C and D). In these experiments, cells were applied in the one chamber and S1P was added in the other chamber. In this device, a narrow plateau between the chambers generates a linear gradient experienced by the cells on the opposite side of the chemokine-filled chamber, and the motility of the cells can be assessed throughout

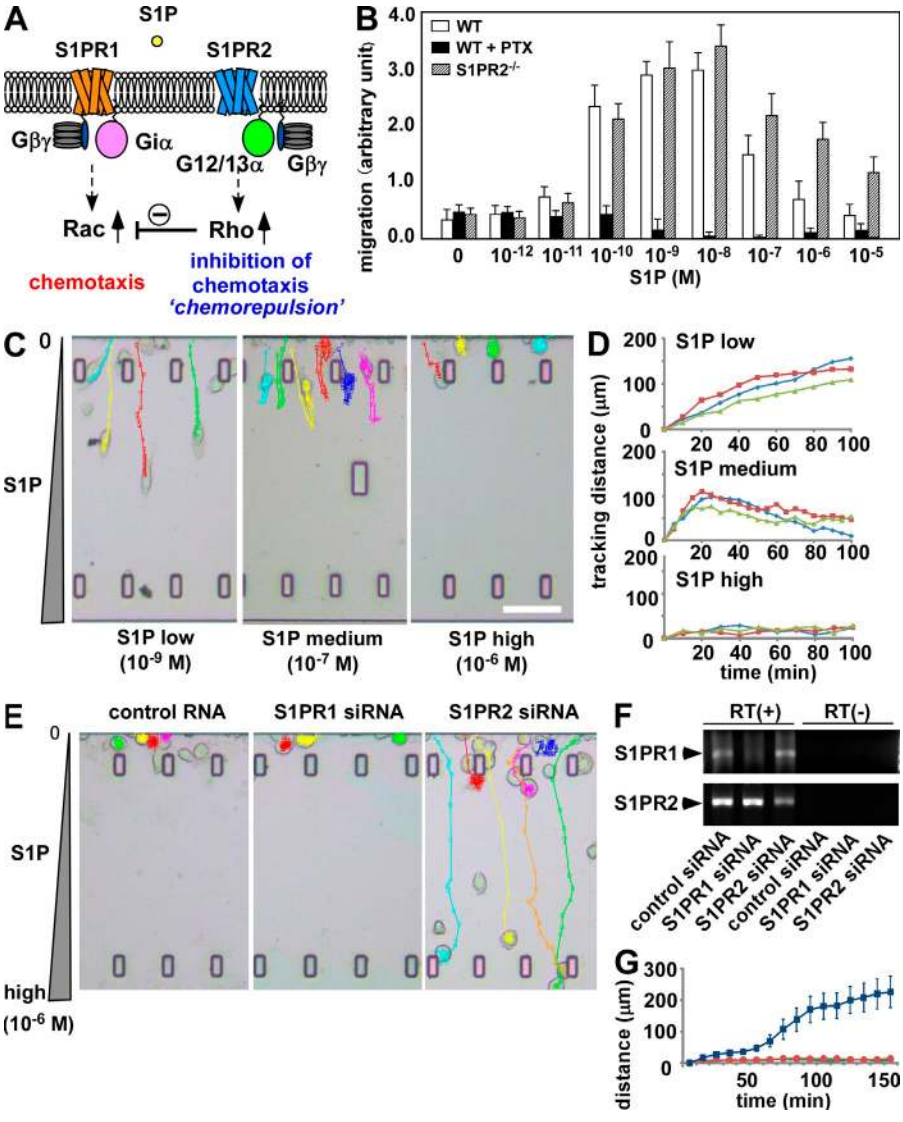

Figure 1. Reciprocal control of S1P chemotaxis by counteracting the receptors S1PR1 and S1PR2. (A) Scheme of function and signal transduction of S1PR1 and S1PR2. (B) In vitro chemotactic response of BM-MDM isolated from wild-type and S1PR2-deficient mice. Before the chemotaxis assay, some cells were treated with 100 nM pertussis toxin (PTX). Error bars represent SD ($n = 6$, from three independent experiments). (C) In vitro S1P-directed chemotaxis of RAW264.7 cells dynamically visualized using EZ-Taxiscan. Cells were loaded in one side of the chamber and the other side was filled with medium containing indicated concentration of S1P (Videos 1–3). Cells migrate into the terrace between the loading chambers. The height from floor to ceiling of the terrace is 8 μm. Bar, 100 μm. (D) Tracking courses from the start line of representative cells in low, medium, and high S1P conditions. Each curve shows the data from one experiment and represents the averaged tracking distance of multiple cells over time. The EZ-Taxiscan experiments were independently performed six times and the data were largely consistent, although the extent of the toward-and-away motions of cells in 10^{-7} M S1P was variable depending on the experiment. Obvious away motion could clearly be observed in five of the six experiments (62 in 83 total cells), and the cells simply stopped in the middle of the chamber without clear backward migration in one of the six experiments (11 in 83 cells). (E) In vitro S1P-directed chemotaxis of RAW264.7 cells treated with siRNAs. Cells pretreated with control RNA duplex, siRNA against S1PR1, or siRNA against S1PR2 (Videos 4–6) were loaded into the EZ-Taxiscan chamber filled with a high concentration of S1P (10^{-9} M) in the other side. (F) RT-PCR detection of S1PR1 and S1PR2 in siRNA-pretreated RAW264.7 cells. Cells were pretreated with control RNA duplex (control siRNA), siRNA against S1PR1 (S1PR1 siRNA), or siRNA against S1PR2 (S1PR2 siRNA). (G) Migration distance data from microscopic analysis of control (red), S1PR1 knockdown (green), and S1PR2 knockdown (blue) cells. The experiments were independently performed three times and the data were largely consistent. Each dot represents the mean value of six independent cells and error bars represent SD.

their exposure to this chemokine gradient in the imaging chamber. RAW264.7 cells, which are often used as a model of OPs, readily migrated toward a low maximal concentration of S1P (10^{-9} M; Fig. 1, C [left] and D [top]; and Video 1) but not toward a high maximal S1P concentration (10^{-6} M; Fig. 1, C [right] and D [bottom]; and Video 3). Strikingly, at an intermediate concentration, cells first moved up the S1P gradient but then arrested this movement and began to migrate back in the opposite direction in nearly all cases (Fig. 1, C [middle] and D [middle]; and Video 2). These data reveal that at high S1P concentrations, RAW264.7 cells respond by chemorepulsion rather than chemoattraction.

RNA interference was used to examine the roles of S1PR1 and S1PR2 in these S1P concentration-dependent behaviors (Fig. 1, E and G). Cells were treated with siRNAs targeting S1PR1 or S1PR2 and put in a high S1P concentration field (10^{-6} M; Fig. 1, E and F). Although control cells and S1PR1 knockdown cells were hardly motile, as observed in Fig. 1 C (Fig. 1, E [left two panels] and G; and Videos 4 and 5), some of the cells treated with siRNA targeting S1PR2 could migrate vigorously, irrespective of the high S1P concentration (Fig. 1, E [right] and G; and Video 6). We also confirmed that S1PR2-deficient primary cultured OPs can efficiently move toward a high S1P concentration (Fig. S1), establishing that S1PR2 expressed on OPs is indeed functional and that this receptor is responsible for the chemorepulsive behavior of these cells (Fig. 1, B and C). These results clearly demonstrate that OPs express two counteracting receptors for S1P: forward movement, promoting S1PR1, and backward movement, promoting S1PR2. The migratory behavior of OPs is thus finely regulated by the balance of the reciprocal functions of these two receptors and their differential activity at distinct concentrations of S1P.

To investigate whether S1PR2 affects OP migration in vivo as these in vitro studies would imply, we performed intravital two-photon imaging of calvaria bones (Mazo et al., 2005; Ishii et al., 2009) and examined the migratory behavior of monocytoid cells resident in the marrow spaces, including OPs. We used CX_3CR1-EGFP knockin (heterozygous) mice (Jung et al., 2000; Niess et al., 2005), in which monocyte-lineage cell types predominantly expressed EGFP. We have previously confirmed that TRAP (tartrate-resistant acid phosphate)-positive mature OCs expressed EGFP in these animals (Ishii et al., 2009) and, in addition, we confirmed that $EGFP^+$ cells (but not $EGFP^-$) can efficiently differentiate into OC-like cells in vitro upon stimulation with RANKL (Fig. S2). Both of these results strongly suggest that $EGFP^+$ cells contain OPs.

CX_3CR1-EGFP–positive cells present in BM stromal locations or at the bone surface were generally stationary under control conditions (Fig. 2 A, top; and Video 7). In contrast, a subset of the labeled cells became motile 2 h after the intravenous application of 3 mg/kg JTE013 (Osada et al., 2002), a potent antagonist for the S1PR2 receptor (Fig. 2 A, bottom; and Video 8), with some of the mobilized cells entering the blood circulation. The cell-mobilizing effect of JTE013 was

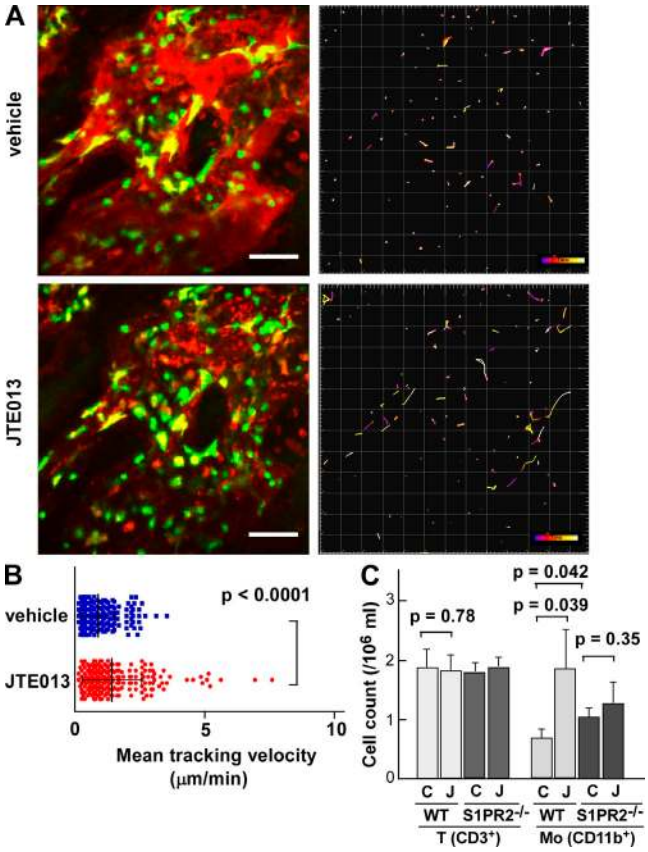

Figure 2. In vivo S1PR2-mediated migration control of OP monocytes visualized using intravital two-photon imaging. (A) Intravital two-photon imaging of mouse skull bone tissues of heterozygous CX_3CR1-EGFP knockin mice, in the absence (vehicle; Video 7) or presence (Video 8) of 3 mg/kg of the S1PR2 antagonist JTE013. CX_3CR1-EGFP–positive cells appear green. The microvasculature was visualized by intravenous injection of 70 kD dextran–conjugated Texas red (red; left). The movements of CX_3CR1-EGFP–positive cells were tracked for 10 min (right). Colored lines show the associated trajectories of cells. Bars, 50 µm. (B) Summary of mean velocity of CX_3CR1-EGFP–positive cells treated with JTE (red circle) or vehicle (blue square). Data points (n = 252 for vehicle and n = 237 for JTE013) represent individual cells compiled from six independent experiments, and error bars represent SD. (C) Effect of the S1PR2 antagonist JTE013 on the composition of peripheral mononuclear cells. Peripheral mononuclear cells collected from wild-type and $S1PR2^{-/-}$ mice administered vehicle (C) or JTE013 (J) were stained with anti-CD3 or anti-CD11b. Absolute numbers of $CD3^+$ T cells or $CD11b^+$ monocytoid cells are described in the figure. Each bar represents the mean value derived from three independent experiments and error bars represent SD.

less pronounced and took longer than was the case with the S1PR1 agonist SEW2871 (Ishii et al., 2009), although the effect was statistically significant (Fig. 2 B). Data collected using larger imaging fields revealed that there was a significant heterogeneity in cellular dynamics that correlated with location of the cells within the BM cavity (Fig. S2 and Video 9). CX_3CR1-$EGFP^+$ cells positioned at the bone surface hardly move, suggesting that these cells have already committed to OC differentiation. In contrast, cells in the parenchyma move after application of JTE013 and, more importantly, the migratory

activities of cells around sinusoids are significantly higher than those of cells in the parenchyma around large collecting venules. Together, these findings suggest that sinusoids are the plausible locations for mobilization of these cells.

Consistent with these findings, we also observed an elevated percentage and absolute number of monocytoid cells in peripheral blood from JTE013-treated mice (Fig. 2 C). This phenomenon was largely absent in S1PR2-deficient mice, suggesting that the effect of JTE013 is exclusively mediated by S1PR2. These results are consistent with the idea that an S1PR2 antagonist can block OP chemorepulsion mediated by the high S1P concentration in blood vessels, facilitating the recirculation of OPs.

To evaluate the in vivo impact of such S1PR2-mediated chemorepulsion of OPs on bone remodeling, we examined mice deficient in S1PR2 (Kono et al., 2004). Morphohistometric analyses using μCT showed that femora of mice genotyped as S1PR2 were moderately osteopetrotic, compared with those of control littermates (Fig. 3 A). Bone tissue density (Fig. 3 B, B.V./T.V.) of S1PR2$^{-/-}$ mice was significantly higher than that of controls, and concordantly trabecular density (Fig. 3 B, Tb.N.) was increased in S1PR2$^{-/-}$ bones. Conventional bone morphohistometrical analyses demonstrated a significant decrease in osteoclastic bone resorption (Fig. 3 C, E.S./B.S.) in S1PR2$^{-/-}$ bones, whereas osteoblast formation was not significantly affected. These results clearly suggest that OC attachment to and function on the bone surface was impaired in S1PR2$^{-/-}$ animals, leading to reduced bone resorption and moderate osteopetrosis. Because the expression of S1PR2 is high in monocytoid OPs and is hardly detected in osteoblast-lineage cells (unpublished data), and because S1PR2 deficiency did not alter the capacity of OP to differentiate into OCs (Fig. S1), this result indicates that S1PR2-mediated chemorepulsion of OPs in response to the high blood S1P concentration contributes to their localization at the bone surface and promotes osteoclastogenesis in vivo.

This newly revealed role of S1PR2-mediated control of OP migration prompted us to examine their therapeutic implications. i.p. administration of RANKL induces substantial osteoporosis within 2 d (Tomimori et al., 2009). We added daily administration of 3 mg/kg of the S1PR2 antagonist JTE013 to this regimen and examined the effect on bone mineral density (Fig. 3 C). Addition of JTE013 significantly reversed the bone density loss induced by RANKL administration (Fig. 3 C, left) by limiting osteoclastic bone resorption (Fig. 3 C, right, E.S./B.S.). This therapeutic effect of JTE013 was absent in S1PR2-deficient mice, suggesting that the function of JTE013 is dependent on this receptor. We also tested the effect of JTE013 by using ovariectomized mice, a conventional model for postmenopausal osteoporosis, and confirmed the significant therapeutic potentials (Fig. S3).

We have previously shown that the S1P–S1PR1 axis contributes to recirculation of OPs into the blood stream (thus acting as a circulation-attractive factor), whereas bone-attractive factors have not been fully elucidated. In this study,

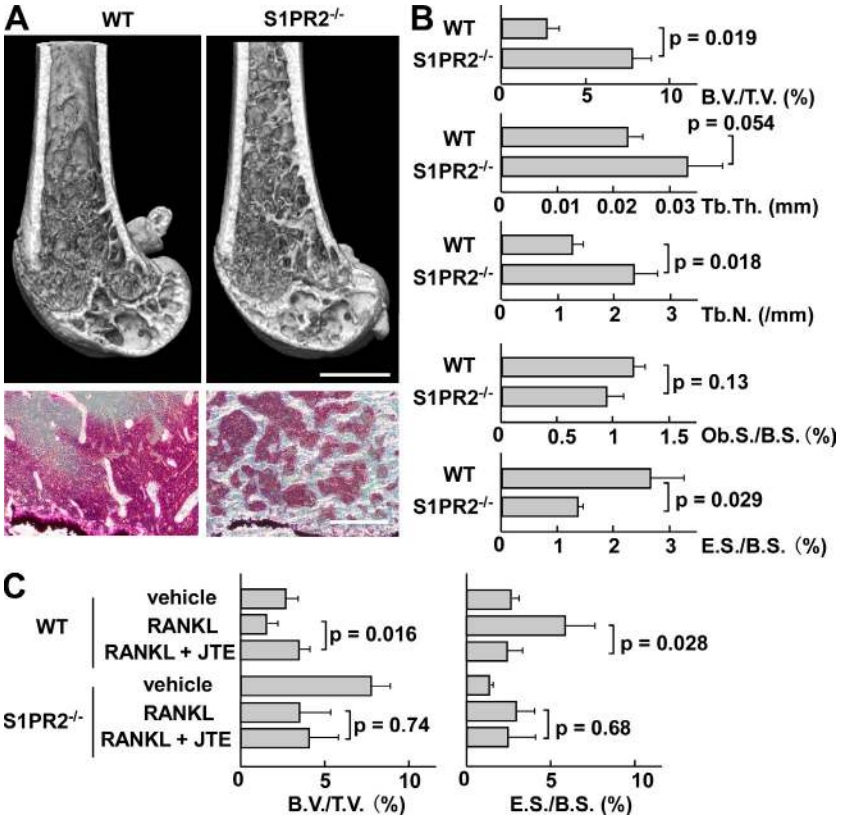

Figure 3. In vivo impact of S1PR2 on bone remodeling. (A) Morphohistometric analyses of control and S1PR2-deficient (S1PR2$^{-/-}$) littermates. Femoral bone samples were analyzed by cone-beam μCT (top) and conventional histological examination (bottom). Bars: (top) 1 mm; (bottom) 200 μm. (B) Summary of the data of bone matrix density (bone volume/tissue volume = B.V./T.V.), trabecular thickness (Tb.Th.), trabecular density (Tb.N.; calculated from μCT images), osteoblast surface per bone surface (Ob.S./B.S.), and osteoclastic erosion surface per bone surface (E.S./B.S.; calculated by conventional morphohistometrical analyses). Error bars represent SD. $n = 3$ for each (from three littermates). (C) Therapeutic effect of S1PR2 antagonist JTE013 on osteoclastic bone resorptive changes. Femurs were collected from each mouse (wild-type and S1PR2$^{-/-}$) after three different treatments: PBS + vehicle, RANKL + vehicle, and RANKL + JTE013. RANKL was dissolved in PBS, and JTE013 was dissolved in a vehicle (PBS containing 5% acidified DMSO and 3% fatty acid–free BSA). Mice were i.p. injected with PBS or RANKL, and with JTE or vehicle, every day for 2 d. Bone samples were analyzed by cone-beam μCT and conventional morphohistological examination. Data of bone matrix density (B.V./T.V.) calculated from μCT images (left) and osteoclastic erosion surface per bone surface (E.S./B.S.) calculated by conventional morphohistometrical analyses (right) were shown. Error bars represent SD. $n = 3$ for each (from three littermates).

we demonstrate a complex regulatory system in which S1P also acts as a bone attractant in certain conditions (actually functioning as a circulation repellant) through a different cognate receptor, S1PR2. In contrast to several chemokines that have already been reported to be important for OP localization, such as CCL2 (Binder et al., 2009), CCL9 (Yang et al., 2006), CXCL1 (Onan et al., 2009), and CXCL12 (Gronthos and Zannettino, 2007), we assume that the S1P–S1PR1/S1PR2 reciprocal axes contribute to regulating the initial entry/exit of OPs across the border of BM vasculature, rather than attachment at the bone surface by itself.

Given these data, we suggest the following model for S1P-mediated localization control of OPs in bone tissues in vivo (Fig. S3). As with other tissues and organs, the S1P concentration in bone tissues is relatively low (Maeda et al., 2010), forming a substantial S1P gradient between BM tissues (parenchyma), the sinusoids, and blood vessels, which is a prerequisite for S1P chemotaxis in situ. Because S1PR1 is readily down-regulated by endocytosis in a high S1P environment, OPs in blood vessels could enter into bones by S1PR2-mediated repulsion, although S1PR2-mediated OP entry into BM has not been fully demonstrated in the present experiments. In addition, we do not assume this is the only mechanism regulating OP entry but rather consider several bone-enriched chemokines, CXCL12 chief among them (Gronthos and Zannettino, 2007), to also be involved in bone recruitment, with S1PR2-mediated chemorepulsion facilitating this process. Once they entered into the parenchyma, S1PR1 would be reexpressed on the cell surface, prompting potential reentry into the circulation if other factors (chemokines and adhesion molecules) at the bone surface do not override this chemoattractive effect. Although it cannot be measured precisely, S1P concentration in BM sinusoids, because of leakage across endothelial barriers, might be expected to be intermediate between parenchymal tissues and blood vessels. If this is the case, it is plausible that OPs can exit from bone tissue via the sinusoids, whose S1P concentration can only activate S1PR1 but not S1PR2. The concept that sinusoids are the place of OP mobilization agrees with our observation that sinusoidal cells have high motility in JTE-treated BM (Fig. S2).

This study clearly demonstrates that reciprocal actions of two S1P receptors regulate the steady-state migration propensities of OPs, constituting a versatile cycle that may play a crucial role in control of osteoclastogenesis and bone remodeling. Although therapeutics in bone-resorptive disorders have so far been targeted mature OCs (such as bisphosphonates) or late OPs fairly committed to OC differentiation (such as denosumab, i.e., anti-RANKL neutralizing antibody), treatment targeting monocytoid early OPs, such as S1P modulators, might be promising as a novel line of treatment in these disorders.

MATERIALS AND METHODS

Cell culture. RAW264.7, a mouse macrophage/monocyte lineage cell line, and mouse BM-derived M-CSF–dependent monocytes (BM-MDM), containing OP cells, were cultured as previously described (Ishii et al., 2006). To stimulate osteoclastogenesis, 50 ng/ml RANKL (PeproTech) was added to the medium and the cells were incubated for 3–4 d. In some experiments, cell were pretreated with siRNAs targeting S1PR1 or S1PR2 (ON-TARGET plus siRNA library; Thermo Fisher Scientific) using a conventional transfection reagent (Lipofectamine 2000; Invitrogen).

In vitro chemotaxis chamber assay. Chemotactic migration of cells was measured in a modified Boyden chamber as described previously (Okamoto et al., 2000).

EZ-Taxiscan chemotaxis assay. Chemotaxis experiments were also conducted in an EZ-Taxiscan chamber according to the manufacturer's protocol (Effector Cell Institute). The EZ-Taxiscan is a visually accessible chemotactic chamber, in which one compartment, containing ligand (S1P), and another compartment, containing cells, are connected by a microchannel. A stable concentration gradient of chemoattractant can be reproducibly formed and maintained through the channel without medium flow. Phase-contrast images of migrating cells were acquired at 1-min intervals. Sequential image data were processed with ImageJ (National Institutes of Health [NIH]), equipped with an add-on program, MT Track J.

Mice. C57BL/6 mice and CX_3CR1-EGFP knockin mice (Jung et al., 2000) were obtained from The Jackson Laboratory. *S1PR2*-defiicient mice (Kono et al., 2004) were obtained from R.L. Proia (National Institute of Diabetes and Digestive and Kidney Diseases, NIH, Bethesda, MD). All mice were bred and maintained under specific pathogen-free conditions at animal facilities of NIH and Osaka University, and all the animal experiments were performed according to NIH institutional guidelines and Osaka University animal experimental guidelines under approved protocols. Mutant mice were genotyped by PCR. All mice were housed and handled according to the institutional guidelines under approved protocols.

Two-photon intravital bone tissue imaging. Intravital microscopy of mouse calvaria bone tissues was performed using a protocol modified from a previous study (Ishii et al., 2009). Mice were anesthetized with isoflurane (Escain; 2.5% vaporized in an 80:20 mixture of O_2 and air), and the hair in the neck and scalp was removed with hair removal lotion (Epilat). The frontoparietal skull was exposed and the mouse head was immobilized in a custom-made stereotactic holder. A catheter was placed into the tail vein with a 30-gauge needle attached to PE-10 tubing (BD). The imaging system was composed of a multiphoton microscope (SP5; Leica) driven by a laser (MaiTai HP Ti:Sapphire; Spectraphysics) tuned to 880 nm and an upright microscope (DM6000B; Leica) equipped with a 20× water immersion objective (HCX APO, N.A. 1.0; Leica). The microscope was enclosed in an environmental chamber in which anesthetized mice were warmed by heated air. Fluorescent cells were detected through a bandpass emission filter at 525/50 nm (for EGFP). Vessels were visualized by injecting 70 kD of Texas red–conjugated dextran (detected using a 650/50 nm filter) i.v. immediately before imaging. In some experiments, 3 mg/kg JTE013 (Tocris Bioscience) dissolved in a vehicle (PBS containing 5% acidified DMSO and 3% fatty acid–free BSA) or vehicle only was injected during the imaging. Image stacks were collected at a 3-µm vertical step size at a depth of 100–150 µm below the skull bone surface. For 3D videos, four sequential image stacks were acquired at 3-µm z spacing to cover a volume of 154 µm × 154 µm × 9.0 µm. The time resolution was 1 min. Raw imaging data were processed with Imaris (Bitplane) with a Gaussian filter for noise reduction. Automatic 3D object tracking with Imaris Spots was aided with manual corrections to retrieve cell spatial coordinates over time.

Mouse treatment experiment. Nine 8-wk-old female, wild-type, or $S1PR2^{-/-}$ mice were injected i.p. with PBS, 2 mg/kg GST-RANKL dissolved in PBS (Tomimori et al., 2009), and 2 mg/kg GST-RANKL and 3 mg/kg JTE013 (dissolved in PBS containing 5% acidified DMSO and 3% fatty acid-free BSA) for 2 d. The mice were then sacrificed and femurs were excised and subjected to histomorphometrical analyses.

Histomorphometry of bone tissues. Trabecular bone morphometry within the metaphyseal region of distal femur was quantified using micro-CT

(ScanXmate-RX; Comscantechno Inc.). 3D microstructural image data were reconstructed, and structural indices, such as B.V./T.V., Tb.Th., and Tb.N., were calculated using TRI/3D-BON software (RATOC Systems). Bone morphometric analysis was performed as previously described (Parfitt et al., 1987).

Flow cytometry. All reagents were purchased from BD. To examine the composition of peripheral blood mononuclear cells, blood was collected from the retroorbital plexus with a heparinized glass pipette from mice treated i.p. 2 h previously with 3 mg/kg JTE013 or vehicle. After removing the red blood cells by ACK lysis buffer (Invitrogen), cells were stained with FITC-conjugated anti-CD11b and PE-Cy7–conjugated anti-CD3, using conventional methods. Flow cytometric data were collected on a FACSCanto II (BD) and analyzed with FlowJo software (Tree Star, Inc.).

Statistics. The Mann-Whitney rank sum test was used to calculate p-values for highly skewed distributions. For Gaussian-like distributions, two-tailed Student's *t* tests were used.

Online supplemental material. Fig. S1 shows chemotaxis and in vitro osteoclastogenesis of S1PR2 knockout OPs. Fig. S2 shows in vivo S1PR2-mediated migration control of CX_3CR1^+ OP monocytes visualized using intravital two-photon imaging. Fig. S3 shows the therapeutic effect of S1PR2 antagonist JTE013 on ovariectomy-induced osteoporosis and schematic model for S1P-mediated localization control of OPs in bone tissues. Videos 1–6 show in vitro chemotaxis of RAW264.7 cells toward an S1P gradient detected using the EZ-Taxiscan device. Videos 7 and 8 show intravital two-photon imaging of mouse skull bone tissues of CX_3CR1-EGFP hetero knockin mice. Video 9 shows intravital two-photon imaging (broad visual field) of mouse skull bone tissues of CX_3CR1-EGFP heterozygous knockin mice. Online supplemental material is available at http://www.jem.org/cgi/content/full/jem.20101474/DC1.

We thank Dr. Richard L. Proia (National Institute of Diabetes and Digestive and Kidney Diseases, National Institutes of Health [NIH]) for S1PR2-deficient mice.

This work was supported in part by the Intramural Research Program of the National Institute of Allergy and Infectious Diseases, NIH, United States Department of Health and Human Services (R.N. Germain), by grants from the International Human Frontier Science Program (LT-00387/2006-L and CDA-00059/2009; to M. Ishii), by a Grants-in-Aid for Encouragement of Young Scientists (A; 22689030), for Scientific Research on Innovative Areas (22113007; to M. Ishii), and a Funding Program for World-Leading Innovative R&D on Science and Technology (FIRST Program) from the Ministry of Education, Science, Sports and Culture of Japan, by Grants-in-Aid for Research on Allergic Disease and Immunology (H21-010; to M. Ishii) from the Ministry of Health, Labor and Welfare of Japan, and by Grants from Takeda Science Foundation (to M. Ishii), from Japan Research Foundation for Clinical Pharmacology (to M. Ishii), from Senri Lifescience Foundation (to M. Ishii), and from Mochida Memorial Foundation for Medical and Pharmaceutical Research (to M. Ishii).

The authors declare no competing financial interests.

Submitted: 22 July 2010
Accepted: 10 November 2010

REFERENCES

Binder, N.B., B. Niederreiter, O. Hoffmann, R. Stange, T. Pap, T.M. Stulnig, M. Mack, R.G. Erben, J.S. Smolen, and K. Redlich. 2009. Estrogen-dependent and C-C chemokine receptor-2-dependent pathways determine osteoclast behavior in osteoporosis. *Nat. Med.* 15:417–424. doi:10.1038/nm.1945

Gronthos, S., and A.C. Zannettino. 2007. The role of the chemokine CXCL12 in osteoclastogenesis. *Trends Endocrinol. Metab.* 18:108–113. doi:10.1016/j.tem.2007.02.002

Ishii, M., K. Iwai, M. Koike, S. Ohshima, E. Kudo-Tanaka, T. Ishii, T. Mima, Y. Katada, K. Miyatake, Y. Uchiyama, and Y. Saeki. 2006. RANKL-induced expression of tetraspanin CD9 in lipid raft membrane microdomain is essential for cell fusion during osteoclastogenesis. *J. Bone Miner. Res.* 21:965–976. doi:10.1359/jbmr.060308

Ishii, M., J.G. Egen, F. Klauschen, M. Meier-Schellersheim, Y. Saeki, J. Vacher, R.L. Proia, and R.N. Germain. 2009. Sphingosine-1-phosphate mobilizes osteoclast precursors and regulates bone homeostasis. *Nature.* 458:524–528. doi:10.1038/nature07713

Jung, S., J. Aliberti, P. Graemmel, M.J. Sunshine, G.W. Kreutzberg, A. Sher, and D.R. Littman. 2000. Analysis of fractalkine receptor CX_3CR1 function by targeted deletion and green fluorescent protein reporter gene insertion. *Mol. Cell. Biol.* 20:4106–4114. doi:10.1128/MCB.20.11.4106-4114.2000

Karsenty, G., and E.F. Wagner. 2002. Reaching a genetic and molecular understanding of skeletal development. *Dev. Cell.* 2:389–406. doi:10.1016/S1534-5807(02)00157-0

Klauschen, F., M. Ishii, H. Qi, M. Bajénoff, J.G. Egen, R.N. Germain, and M. Meier-Schellersheim. 2009. Quantifying cellular interaction dynamics in 3D fluorescence microscopy data. *Nat. Protoc.* 4:1305–1311. doi:10.1038/nprot.2009.129

Kono, M., Y. Mi, Y. Liu, T. Sasaki, M.L. Allende, Y.P. Wu, T. Yamashita, and R.L. Proia. 2004. The sphingosine-1-phosphate receptors S1P1, S1P2, and S1P3 function coordinately during embryonic angiogenesis. *J. Biol. Chem.* 279:29367–29373. doi:10.1074/jbc.M403937200

Maeda, Y., N. Seki, N. Sato, K. Sugahara, and K. Chiba. 2010. Sphingosine 1-phosphate receptor type 1 regulates egress of mature T cells from mouse bone marrow. *Int. Immunol.* 22:515–525. doi:10.1093/intimm/dxq036

Mazo, I.B., M. Honczarenko, H. Leung, L.L. Cavanagh, R. Bonasio, W. Weninger, K. Engelke, L. Xia, R.P. McEver, P.A. Koni, et al. 2005. Bone marrow is a major reservoir and site of recruitment for central memory $CD8^+$ T cells. *Immunity.* 22:259–270. doi:10.1016/j.immuni.2005.01.008

Niess, J.H., S. Brand, X. Gu, L. Landsman, S. Jung, B.A. McCormick, J.M. Vyas, M. Boes, H.L. Ploegh, J.G. Fox, et al. 2005. CX_3CR1-mediated dendritic cell access to the intestinal lumen and bacterial clearance. *Science.* 307:254–258. doi:10.1126/science.1102901

Okamoto, H., N. Takuwa, T. Yokomizo, N. Sugimoto, S. Sakurada, H. Shigematsu, and Y. Takuwa. 2000. Inhibitory regulation of Rac activation, membrane ruffling, and cell migration by the G protein-coupled sphingosine-1-phosphate receptor EDG5 but not EDG1 or EDG3. *Mol. Cell. Biol.* 20:9247–9261. doi:10.1128/MCB.20.24.9247-9261.2000

Onan, D., E.H. Allan, J.M. Quinn, J.H. Gooi, S. Pompolo, N.A. Sims, M.T. Gillespie, and T.J. Martin. 2009. The chemokine Cxcl1 is a novel target gene of parathyroid hormone (PTH)/PTH-related protein in committed osteoblasts. *Endocrinology.* 150:2244–2253. doi:10.1210/en.2008-1597

Osada, M., Y. Yatomi, T. Ohmori, H. Ikeda, and Y. Ozaki. 2002. Enhancement of sphingosine 1-phosphate-induced migration of vascular endothelial cells and smooth muscle cells by an EDG-5 antagonist. *Biochem. Biophys. Res. Commun.* 299:483–487. doi:10.1016/S0006-291X(02)02671-2

Parfitt, A.M., M.K. Drezner, F.H. Glorieux, J.A. Kanis, H. Malluche, P.J. Meunier, S.M. Ott, and R.R. Recker; Report of the ASBMR Histomorphometry Nomenclature Committee. 1987. Bone histomorphometry: standardization of nomenclature, symbols, and units. *J. Bone Miner. Res.* 2:595–610. doi:10.1002/jbmr.5650020617

Rosen, H., and E.J. Goetzl. 2005. Sphingosine 1-phosphate and its receptors: an autocrine and paracrine network. *Nat. Rev. Immunol.* 5:560–570. doi:10.1038/nri1650

Takuwa, Y. 2002. Subtype-specific differential regulation of Rho family G proteins and cell migration by the Edg family sphingosine-1-phosphate receptors. *Biochim. Biophys. Acta.* 1582:112–120.

Teitelbaum, S.L. 2000. Bone resorption by osteoclasts. *Science.* 289:1504–1508. doi:10.1126/science.289.5484.1504

Teitelbaum, S.L., and F.P. Ross. 2003. Genetic regulation of osteoclast development and function. *Nat. Rev. Genet.* 4:638–649. doi:10.1038/nrg1122

Tomimori, Y., K. Mori, M. Koide, Y. Nakamichi, T. Ninomiya, N. Udagawa, and H. Yasuda. 2009. Evaluation of pharmaceuticals with a novel 50-hour animal model of bone loss. *J. Bone Miner. Res.* 24:1194–1205. doi:10.1359/jbmr.090217

Yang, M., G. Mailhot, C.A. MacKay, A. Mason-Savas, J. Aubin, and P.R. Odgren. 2006. Chemokine and chemokine receptor expression during colony stimulating factor-1-induced osteoclast differentiation in the toothless osteopetrotic rat: a key role for CCL9 (MIP-1γ) in osteoclastogenesis in vivo and in vitro. *Blood.* 107:2262–2270. doi:10.1182/blood-2005-08-3365